THE ASTRONOMICAL JOURNAL VOLUME 86, NUMBER 9 SEPTEMBER 1981

THE MULTIPLE-POINT FRINGE-RATE METHOD OF MAPPING SPECTRAL-LINE VLBI SOURCES WITH APPLICATION TO H_2O MASERS IN W3–IRS5 AND W3(OH)

R. C. WALKER
National Radio Astronomy Observatory,[a] Charlottesville, Virginia 22901
Received 14 May 1981

ABSTRACT

Astrophysical masers often have spatial structures which consist of a small number of well separated, compact features at each frequency. VLBI observations of such structures produce relative fringe-rate spectra which have multiple peaks. Giuffrida has shown that these peaks can be used to produce maps while avoiding some of the worst calibration difficulties of aperture synthesis. The current multiple-point fringe-rate mapping method, along with some of its advantages and limitations, is described in this paper. The method has been used to map the H_2O maser emission in W3–IRS5 and W3(OH). The additional details seen in these maps, compared to previously published observations, make division of the sources into centers of activity difficult.

I. INTRODUCTION

The lack of phase information is a basic difficulty in the construction of an image of a radio source from Very Long Baseline Interferometer (VLBI) data. This difficulty can be overcome for spectral-line data if the brightness distribution at a particular velocity is simple and can be derived without using phase (although closure phase could be used). The data at that velocity are then used as a phase reference. Absolute position information is lost, but images of the emission at other velocities can be formed. Four methods have been used to form such images: (1) the single-point fringe-rate method, (2) model fitting, (3) aperture synthesis, and (4) the multiple-point fringe-rate method. These methods differ significantly in both the accuracy and complexity of the maps they produce, and in the difficulty of the required calibration. The method used in a particular experiment will depend on the goals of the experiment and on the complexity of the sources mapped. It is the purpose of this paper to describe, in detail, the multiple-point fringe-rate method which was developed to its current level of sophistication for the reduction of observations of H_2O masers in W49N made in June 1978 (Walker, Matsakis, and Garcia-Barreto 1981, Paper I). Maps of the H_2O masers in W3–IRS5 and W3(OH), made with data from the same experiment, are presented as examples of multiple-point fringe-rate maps. These maps are more detailed than those from previous observations and suggest that the sources probably do not consist of several centers of activity.

The single-point fringe-rate method (Moran 1976) was used in most observations until recently. For this method, the radiation at each velocity is assumed to come from one point source. The rate of change of phase (fringe rate) as a function of time is used to solve for an offset from the position of the reference feature. The method requires very little calibration. A few experiments have been reduced using aperture synthesis techniques (Reid and Muhleman 1978; Walker *et al.* 1978; Reid *et al.* 1980; Haschick *et al.* 1981), which do not make strong assumptions about the brightness distributions. These experiments have demonstrated that the single point source assumption is very often bad. However, they do show that the emission in an astrophysical maser at a specific velocity tends to come from a small number of compact sources. These experiments have also demonstrated that reduction of spectral-line VLBI data using aperture synthesis is a difficult and time-consuming task. Model fitting has been used primarily to derive very accurate relative positions of features which are assumed to be point sources (Moran 1976; Reid *et al.* 1977). It is either limited to the single point source assumption used in the early fringe-rate technique, or subject to many of the difficulties of aperture synthesis.

The multiple-point fringe-rate method is an alternative mapping technique which takes advantage of the typical multiple-point nature of astrophysical masers, while avoiding some of the most difficult problems of aperture synthesis. It was originally developed by Guiffrida (1977) to study a flaring feature in W3(OH).

II. THE METHOD

The fringe-rate mapping methods use the fact that the fringe rate, or rate of change of phase, ω_f, for a feature offset from the phase center of the data by the angular coordinates, x and y, is given by

$$\omega_f = 2\pi(x\, du/dt + y\, dv/dt), \quad (1)$$

where u and v are the projected baseline components in units of wavelengths. The phase center is usually estab-

[a]The National Radio Astronomy Observatory is operated by Associated Universities, Inc., under contract with the National Science Foundation.

lished by a reference feature. A fringe-rate spectrum may be obtained by performing a Fourier transform on a time sequence of amplitude and phase data. For simplicity, each such time sequence, which is typically a few minutes or tens of minutes long, will be called a scan. If a peak is found in a fringe-rate spectrum at a value ω_f, Eq. (1) gives a line on the sky along which the emission corresponding to the peak must lie. Since du/dt and dv/dt change with time, it is possible to find the position of the emission by finding the point at which the lines corresponding to different scans intersect. This can be done formally by a least-squares fit to the data (ω_f) for the position offset (x,y), given the known geometric parameters (du/dt and dv/dt).

If there is emission at the same velocity at several locations, several fringe-rate peaks, one corresponding to each location, will be produced for each scan. The peaks will occasionally be blended when two emission locations happen to produce similar fringe rates. The object of the multiple-point fringe-rate method is to utilize the peaks in the fringe-rate spectra of a number of scans to find the different locations of emission features. There are several ways this could be done. The choice of a technique is governed by the following constraints: (1) the technique should be tolerant of spurious peaks in some scans; (2) it should not require that peaks corresponding to all features appear in all scans; (3) it should not use a map grid; (4) it should be as immune as possible to finding false features; and (5) the derived feature positions should be as accurate as the data will allow. The first two constraints allow the use of data of low or variable signal-to-noise. The third constraint is a consequence of the huge arrays that would be needed to map features separated by arcseconds with a resolution of a milliarcsecond or less as in a typical H_2O experiment. The method currently in use is described below.

First the data must be calibrated. The calibration of spectral-line VLBI data is described in the Appendix to Reid *et al.* (1980). The major calibration steps are to: (1) correct for the bandpass response function of each telescope, (2) shift all spectra to a common center velocity, (3) reference the phases to a spectral feature whose spatial distribution is well understood, (4) correct phase slopes caused by delay (usually clock) errors in the initial processing, and (5) calibrate the amplitudes using the total-power spectra from each telescope. All of these calibrations are required for modeling or for aperture synthesis. The fringe-rate methods are not sensitive to constant phase offsets and so do not require what is often one of the hardest calibration tasks—the removal of phase slopes. In fact, the single-point fringe-rate method is often used without any calibration, except phase referencing, since the largest peak in a fringe-rate spectrum of even uncalibrated data is almost certainly due to the most intense spatial feature at the velocity of the spectrum. If the multiple-point fringe-rate method is to be used, all the calibration steps except (4) should be done.

After calibration, the data from each scan are Fourier transformed to form the fringe-rate spectrum of each velocity channel. The choice of the length of a scan involves a trade-off of fringe-rate resolution and sensitivity against field of view. The error in a derived fringe rate decreases with the 3/2 power of the integration time (Moran 1973) so the accuracy of derived positions of emission features is greatly enhanced by long integration times. The fringe-rate resolution also increases with integration time, which can be valuable if there are closely spaced peaks. Finally, the sensitivity for the detection of weak features increases with the square root of the integration time. However, the fringe rate of a feature offset from the phase center changes with time, since du/dt and dv/dt change with time. This will smear the peak due to a feature with a large offset and make the fit for an accurate position difficult. The smearing is given approximately by

$$\frac{d\omega_f}{dt}\Delta t = 2\pi\left(\frac{d^2u}{dt^2}x + \frac{d^2v}{dt^2}y\right)\Delta t, \tag{2}$$

where Δt is the length of a scan. If we want the smearing to be kept to a value on the order of the fringe-rate resolution, which is about $1/\Delta t$, we require

$$(d\omega_f/dt)\,\Delta t < 1/\Delta t, \tag{3}$$

or

$$\frac{d^2u}{dt^2}x + \frac{d^2v}{dt^2}y < \frac{1}{2\pi\Delta t^2}. \tag{4}$$

The accuracy with which fringe rates can be determined depends on the signal-to-noise of the data, while the degree of smearing that can be tolerated depends on the desired accuracy of the final source positions, so the above constraint is not precise. It is often convenient to use a rectangular field of view, or window, defined by

$$|x| < \min\left[\left(2\pi\Delta t^2\frac{d^2u}{dt^2}\right)^{-1}\right],$$
$$|y| < \min\left[\left(2\pi\Delta t^2\frac{d^2v}{dt^2}\right)^{-1}\right], \tag{5}$$

where the minimum is taken over all scans contributing to the map, and where increased smearing for features in the corners is tolerated.

The size of the window can be adjusted either by altering the constraint on the smearing or by changing the integration time. The length of a scan must be chosen based on the nature of the source and the goals of the experiment. If one is forced to use a window that is smaller than the total extent of the source, the whole region can be mapped by making several maps with phase centers offset from the reference feature. This was done for the maps presented later in this paper and for the map of W49N presented in Paper I.

Once the fringe-rate spectra are obtained, the separate fringe-rate peaks are located and an interpolated amplitude and rate are obtained for each one. Care must be taken to distinguish between noise peaks and real peaks due to emission features. This is done in our pro-

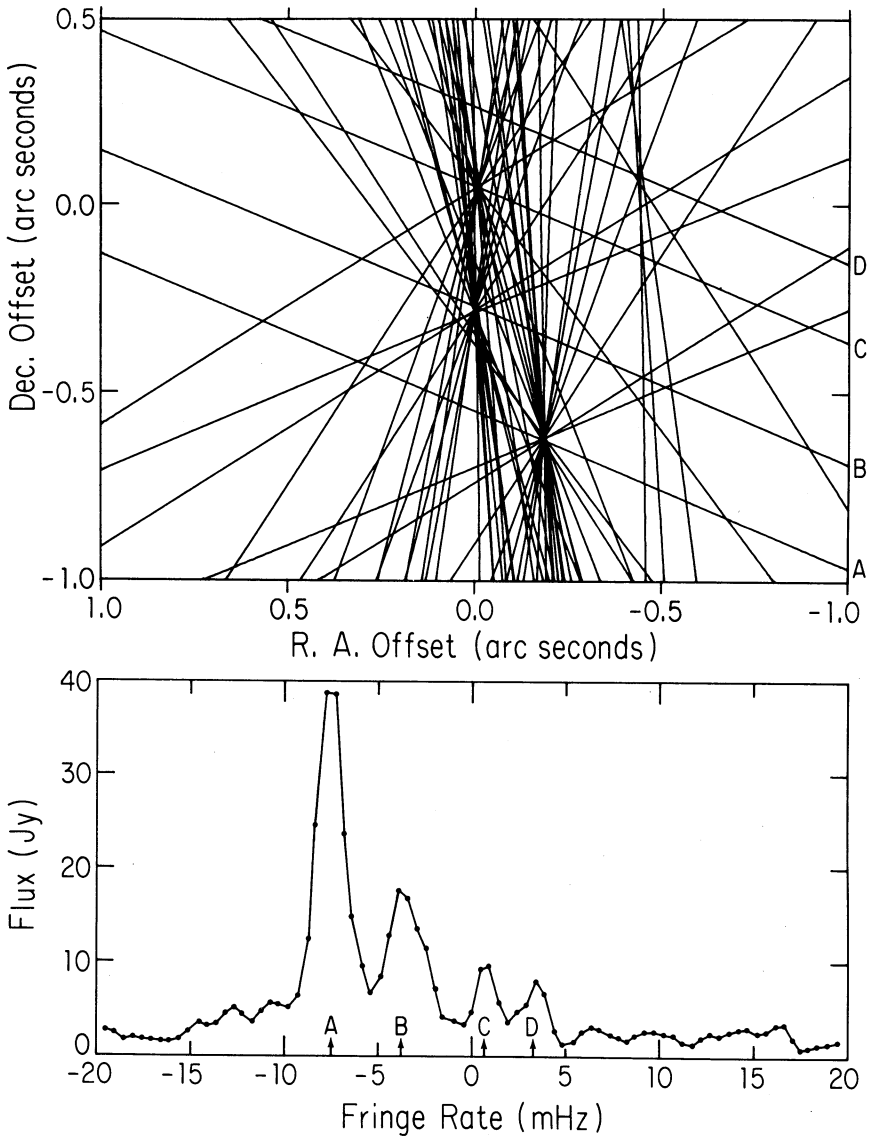

FIG. 1. The lower plot is a fringe-rate spectrum of one velocity channel from one scan for the source W49N. There are four peaks, each corresponding to a separate feature on the sky. Each peak confines its corresponding feature to lie along a line on the sky. The upper plot shows such lines from many scans. The peaks in the lower plot and their corresponding lines in the upper plot are labeled A–D. There are clearly four separate features at the velocity of these data, including one (corresponding to line D) that is sufficiently far from the phase center so that smearing of the fringe-rate peaks will prevent derivation of an accurate position. The window in which reasonable positions can be found is about 0".5 in R.A. by 2".0 in Decl. for this low-declination source with 20-min integrations. The window can be moved by shifting the phase center of the data.

grams by requiring each peak to be larger than a factor *a* times the rms amplitude of data not in peaks, and by requiring that two blended peaks be separated by a dip of a factor *b* times the same rms amplitude. The factors *a* and *b* can be chosen by the user and are typically 3.5–5, depending on the number of points in the spectra and on the quality of the data.

The current programs obtain the interpolated amplitude and rate of each each peak by using a quadratic solution of the three highest points of the peak. The fringe-rate spectra used for the interpolation should be produced from data arrays of complex fringe amplitude versus time, which have been padded with zeros to at least 3/2 their original length. The points in such "over-resolved" spectra are correlated, which greatly improves the accuracy of the interpolation. For data with a high signal-to-noise ratio and sufficiently over-resolved spectra, this interpolation procedure should not introduce significant errors. For low signal-to-noise data, however, errors on the order of the fringe-rate resolution may be introduced. A more complex, nonlinear fitting procedure would help in such cases and will be tried soon.

The interpolated fringe rates can be used to form line plots such as the example in Fig. 1. This example shows how the mapping works and shows some of the problems that are encountered. It is clear that the velocity channel for which the plot was made contains four spatial features, including one (feature D) which is outside the window and shows a poorly defined location owing to smearing. A computer program that finds and fits for the location of the features must be able to select the

lines (fringe-rate peaks) which go with each feature, and must be able to reject intersections that do not correspond to a feature. The program we use to accomplish this task uses the following procedure. A few of the best scans are selected by the observer to serve as the starting points for the search for features. The first line from the first selected scan is examined for the location of the highest density of intersections with the lines from all other scans. All lines passing within a specified distance of this location are used to fit for a feature position. The distance is specified in terms of the sensitivity of the fringe rate corresponding to the line, and to position offsets, and is different for each line. The worst fringe rates in the fit are then rejected and the fit is repeated. This iteration procedure is continued until the fit is considered good enough, there are too few lines left, or a maximum number of iterations is reached. The program then returns to the second line in the first selected scan and repeats the process. This is continued until all lines in the selected scans are exhausted. Throughout the process, lines which have been used in a previous fit cannot be used in finding the location to begin a new fit. However, they can be used in the new fit if they lie sufficiently close to the starting location. In addition, in later cycles, a check is made to ensure that the new point is not the same as one found earlier. This whole process is repeated for each velocity channel.

The program works reasonably well but it can still be confused, especially when features lie close together. It is wise to examine the line plots, such as Fig. 1, for channels spaced closely enough so that each map feature is seen in a plot. For data such as those presented in this paper and in Paper I, where nearly every feature appeared in at least two or three channels, plots for every other channel were examined. Since people are adept at the pattern recognition task required to select features, this procedure should almost completely eliminate spurious features.

Each maser feature will generally appear in several channel maps at adjacent velocities. The data from the maps are used to solve for the feature position, flux density, and velocity. These are the values that are used to make the final maps. The channel map data can also be used to derive spectra of the emission within a specified region on the sky, simply by adding all points that belong to features whose mean position lies within the region.

Any spectra or flux densities derived from the maps should be treated with caution. The flux density of a map feature is simply the average of the flux density in each of the fringe-rate peaks corresponding to that feature. Therefore, if there is a scan for which two features give peaks at the same fringe rate, the flux of both features will tend to be increased. In addition, if a feature is partially resolved, the flux density in the maps will be reduced. The flux density of an astrophysical maser is very sensitive to small variations in the geometry, velocity field, and pump in a masing region, and therefore, for most experiments, accurate flux densities are not as important as accurate positions and velocities in attempts to understand the overall source structure. If the flux densities are crucial to the experiment, as in studies of flux variations, great care should be taken to avoid the above problems, or the aperture synthesis technique should be used to make maps.

The accuracy of the relative positions of features in the maps, under ideal conditions, can approach that available using phases. However, ideal conditions are seldom obtained. Usually the accuracy of the relative fringe rates used to make the maps is limited by low signal-to-noise ratio, smearing due to large position offsets, confusion or resolution of features, changing phase slopes due to drifting clocks, poor reference feature quality, or insufficiently long scans. If there are several scans, the accuracy of each feature position is given by the formal errors from the least-squares fitting procedure. For most experiments, the errors cover a wide range with typical values on the order of twice the fringe spacing.

III. OBSERVATIONS

Three-station VLBI observations of the H_2O masers in W3–IRS5, W3(OH), and W49N were made on 1978 June 14–16. W49N was the primary target of the experiment and a 386-feature multiple-point fringe-rate map of that source is presented in Paper I. The details of the experiment are also given in Paper I. The stations were the 37-m telescope of the Haystack Observatory in Westford, Massachusetts, the 43-m telescope of the National Radio Astronomy Observatory in Green Bank, West Virginia, and the 40-m telescope of the Owens Valley Radio Observatory in Big Pine, California. All three telescopes were equipped with maser time standards and maser receivers. The data were recorded on the Mark II VLBI system (Clark 1973) at a bandwidth of 2 MHz and processed on the NRAO correlator in Charlottesville, Virginia. For W3(OH), high-velocity features were observed by switching frequencies every second over four separate bands. Maps were produced from the data using the multiple-point fringe-rate method described in Sec. II.

a) W3(OH)

The first use of a multiple-point fringe-rate mapping method (Giuffrida 1977) was part of an effort to study a feature in W3(OH) which flared and decayed in a 36-day period in mid-1977 (Haschick, Burke, and Spencer 1977; Burke, Giuffrida, and Haschick 1978). The total-power spectrum of W3(OH) (Fig. 2) is deceptively simple, apparently consisting of a small number of overlapping features. The VLBI data, however, show that it consists of several spatially separated features at each velocity. In fact, earlier attempts to map the source with aperture synthesis (Walker *et al.* 1978) were frustrated by lack of a reference feature. Only the most general

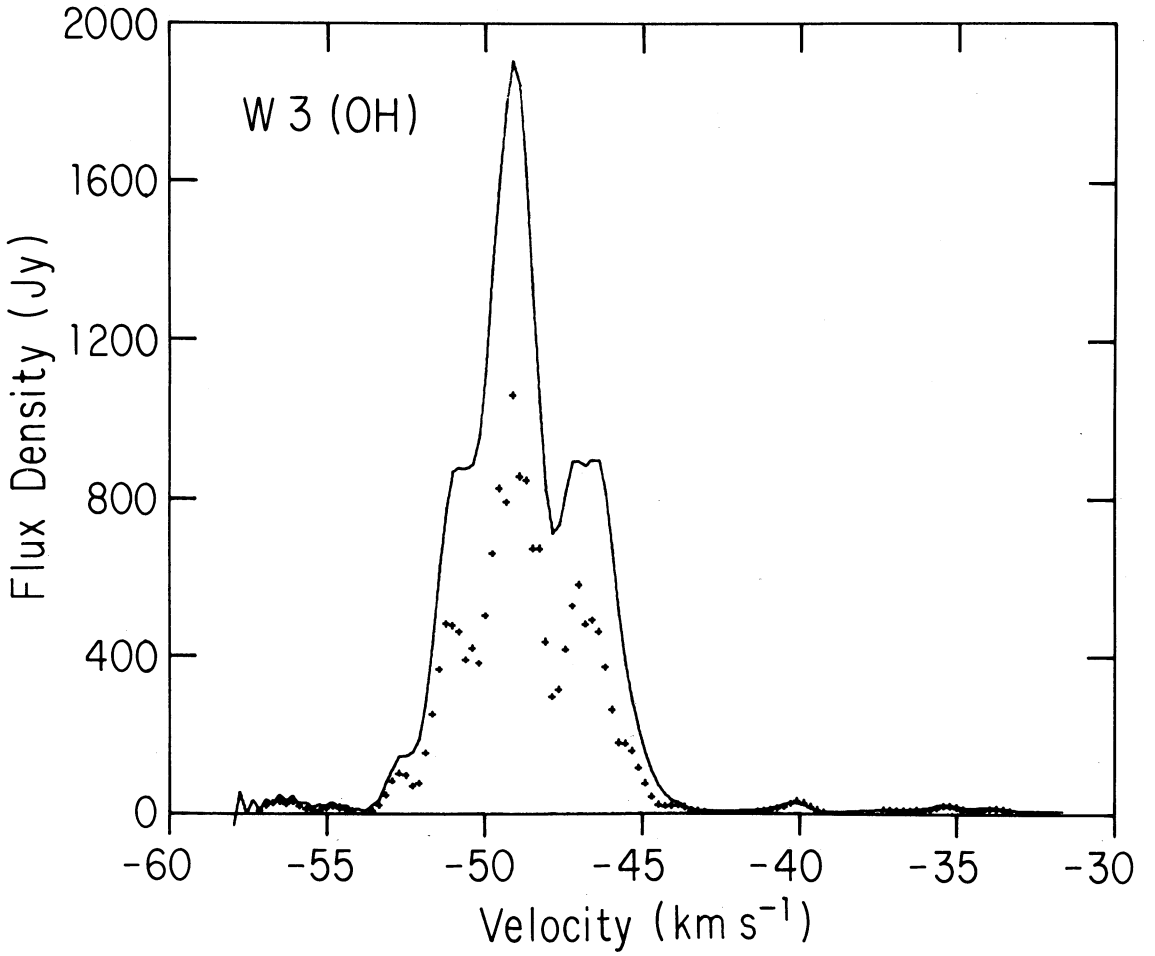

FIG. 2. The total-power spectrum of W3(OH) in June 1978 is shown by a solid curve. The symbols show the sum of the flux densities at each velocity in the map of Fig. 3. The flux density scale may be in error by up to 30%.

characteristics of single-point fringe-rate maps produced from such data can be believed. The multiple-point fringe-rate method was used to separate the flaring feature from the other features at the same velocity.

The map of W3(OH) in June 1978 is presented in Fig. 3. The velocity, flux density, R.A., and Decl. offsets from the reference feature, with their errors, and the total velocity range of each feature are given in Table I. No spectral channel contains a single point source, so a channel containing two widely separated features, one much stronger than the other, was used as a phase reference. A running average phase was used to smear out the effects of the distant feature. The total power in the map of each velocity channel is shown in Fig. 2. The missing flux density presumably represents a combination of confusing features which were not mapped, and partial resolution of some of the map features. The general characteristics of the map agree with previous observations: the source consists of an arc of bright features confined to a region about 0".2 in size which lies at the east end of a 2".0×0".5 group of weak features (Walker *et al.* 1978; Giuffrida 1977; Genzel *et al.* 1978). Four frequency windows, covering the velocity range − 6 to − 105 km s^{-1} were examined, but no features were detected outside of the 2-MHz window covering − 58 to − 31 km s^{-1}.

The map of W3(OH) shows that the weak features in the extended region cover the whole velocity range of the bright knot. The total velocity range of features above our detection limit in the extended region is only 50% larger than in the bright knot, so if these features are "high-velocity features" as discussed by Genzel *et al.* (1978), they must be moving transverse to the line of sight. A reanalysis of old data using the new techniques or astrometric measurements, such as those performed on Orion by Genzel *et al.* (1980), could clarify the nature of these features. Comparison of our map with the maps of Giuffrida (1977) indicates that transverse motions within the bright knot are small (< 10 or 20 km s^{-1}), while two of the outer features may have transverse ve-

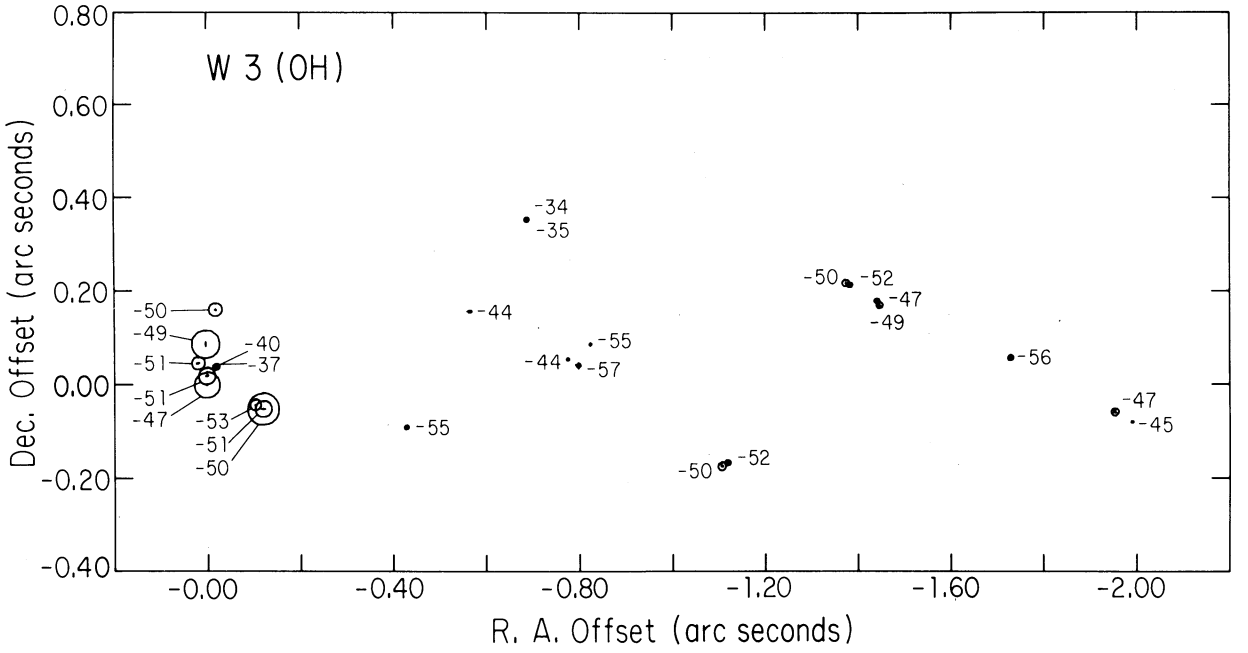

FIG. 3. The map of the H_2O masers in W3(OH). Each feature is marked by a circle whose area is proportional to its flux density and by a cross, the arms of which indicate the one sigma errors in the feature position.

locities of 50–100 km s^{-1} away from the bright knot. However, the data are not of sufficient quality to give conclusive evidence of high-velocity motion. The lack of obvious clustering in the extended regions suggests that the features are associated with the energy source of the bright knot rather than being totally separate.

b) W3–IRS5

The total-power spectrum of W3–IRS5 [sometimes called W3(C) H_2O] is shown in Fig. 4. This source consists of several clearly separated lines, some of which are not confused. A reference feature which is truly point-like was found at -36.8 km s^{-1}. The map of the source is shown in Fig. 5 and the total power in each map channel is shown in Fig. 4. The parameters of each feature are given in Table II. For unconfused features in this source, the missing power probably indicates that the feature is resolved. As for W3(OH), missing power in velocity channels with several features may represent additional, missed features. The map agrees, generally, with previously published results which are summarized by Genzel *et al.* (1978). However, the addition of the features at -42 and -41 km s^{-1} between the centers of activity suggested by Genzel *et al.* (1978) casts some doubt on the suggested clustering. While the most southern features are possibly separate, it seems plausible that the rest of the features are associated with one object. The size of the group, 7×10^{16} cm (assuming distance of 3 kpc), is no larger than other groups of apparently related features in W3(OH) and W49N.

IRS5 is a powerful source of far-infrared radiation

TABLE I. Water masers in W3(OH).

VELOCITY KM S^{-1}	FLUX JY	RA OFFSET 0^m.001		DEC OFFSET 0^m.001		RANGE KM S^{-1}	VELOCITY KM S^{-1}	FLUX JY	RA OFFSET 0^m.001		DEC OFFSET 0^m.001		RANGE KM S^{-1}
-56.8	11	-798.2	+-2.0	40.6	+-7.0	2.1	-49.6	730	-120.0	+-4.1	-50.5	+-1.5	3.0
-56.3	22	-1729.7	0.7	56.5	0.7	1.7	-48.7	30	-1447.6	0.8	169.7	2.0	0.8
-54.8	12	-428.2	0.4	-89.9	0.7	1.1	-48.7	576	3.4	0.5	87.6	5.0	2.7
-54.8	4	-823.2	1.9	85.8	4.2	0.8	-47.1	41	-1953.4	0.4	-58.3	0.8	1.1
-52.7	86	-102.9	0.3	-41.7	0.1	1.5	-46.6	471	0.5	0.5	0.4	0.6	4.8
-52.0	25	-1118.4	0.7	-166.4	1.3	1.7	-46.6	19	-1441.4	0.7	179.4	1.0	0.4
-51.6	21	-1383.1	3.3	213.3	4.5	0.2	-44.9	5	-1990.6	0.7	-80.1	1.0	0.4
-51.2	200	-120.2	0.3	-50.2	0.6	1.5	-43.9	6	-565.1	3.3	156.6	0.8	0.6
-51.1	125	19.2	2.1	47.1	0.7	1.9	-43.8	5	-775.1	1.2	53.4	1.7	1.5
-50.9	205	0.7	1.3	19.5	0.5	1.9	-40.0	28	-19.4	0.5	39.5	0.4	2.3
-50.4	38	-1374.3	0.5	217.3	1.0	0.2	-37.3	1	-22.1	0.1	35.7	0.1	0.2
-50.2	49	-1106.4	0.8	-173.7	0.9	0.4	-35.3	16	-686.5	1.0	353.2	0.9	3.0
-50.0	134	-18.2	1.2	161.5	0.5	0.6	-33.9	8	-686.1	0.6	353.1	0.6	1.3

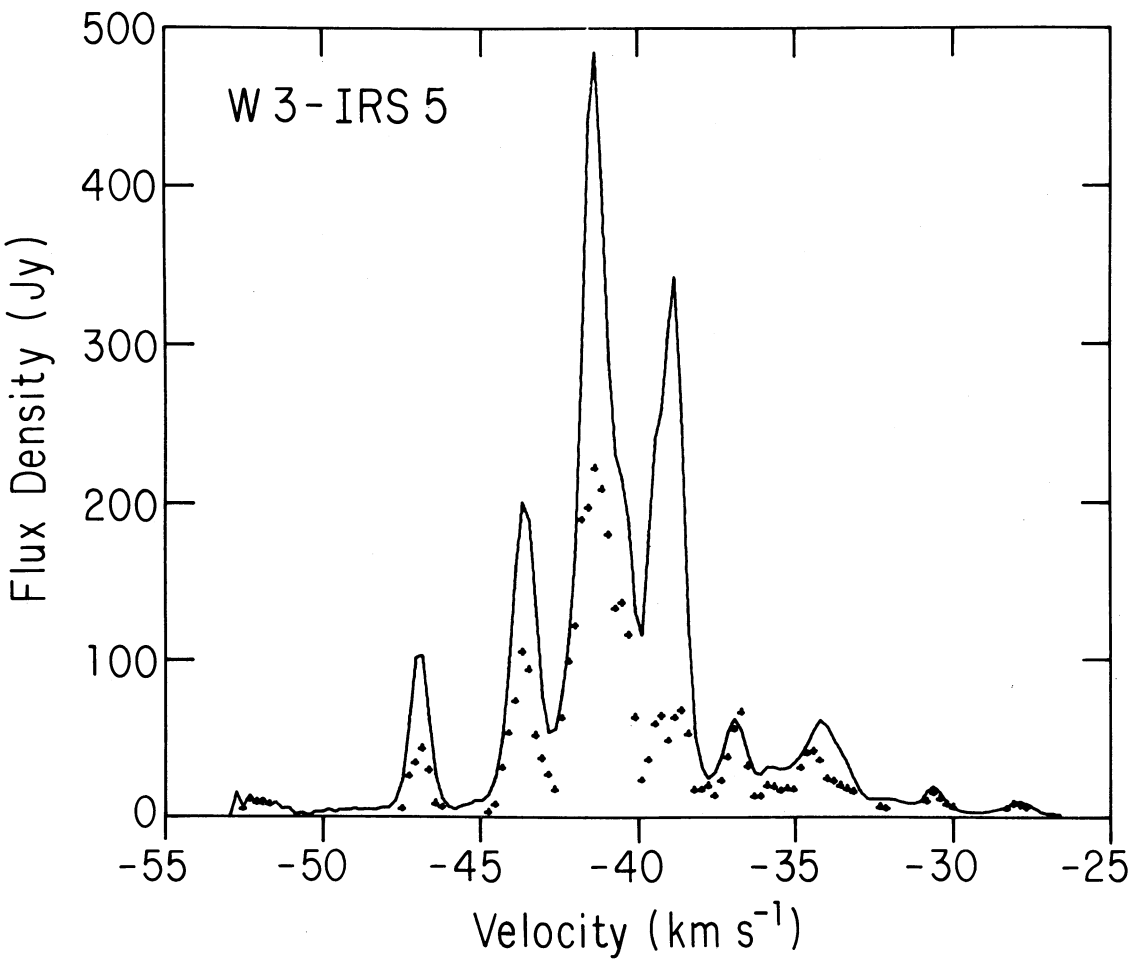

FIG. 4. The total-power spectrum of W3–IRS5 is shown by a solid curve. The symbols show the sum of the flux densities in the features in the map of Fig. 5. As in Fig. 2, the flux density scale should be treated with caution.

TABLE II. Water masers in W3–IRS5.

VELOCITY KM S^{-1}	FLUX JY	RA OFFSET 0".001	DEC OFFSET 0".001	RANGE KM S^{-1}	VELOCITY KM S^{-1}	FLUX JY	RA OFFSET 0".001	DEC OFFSET 0".001	RANGE KM S^{-1}
-52.3	12	193.2+-3.9	1023.1+-3.0	1.1	-40.5	94	206.2+-0.6	-330.4+-0.5	1.1
-46.9	37	-6.4 1.0	130.8 0.3	1.1	-40.4	56	125.6 0.2	1113.5 0.5	1.1
-46.6	12	184.8 1.1	1020.3 1.1	1.3	-39.5	42	-16.4 1.3	893.9 0.5	0.6
-43.7	81	600.8 1.6	977.4 1.1	1.7	-38.7	31	205.8 0.8	-331.0 0.1	1.9
-43.6	27	345.9 2.4	760.7 1.6	2.1	-38.6	37	272.7 0.8	203.3 0.6	1.1
-42.9	6	20.1 4.4	1124.2 0.7	0.4	-36.8	68	0.0 0.5	-0.0 0.1	2.3
-42.4	11	385.4 0.6	410.3 1.1	0.6	-35.8	11	716.6 1.9	-1389.5 1.7	1.1
-42.2	19	362.1 2.1	726.2 0.8	1.1	-34.9	18	0.5 1.2	2.3 0.4	1.7
-42.0	48	300.5 0.8	1068.3 0.9	0.8	-34.2	30	685.6 2.3	-1380.7 1.9	1.9
-41.6	66	35.9 1.4	973.7 0.7	0.4	-32.3	5	701.7 1.1	-1302.2 0.5	0.4
-41.3	145	-20.7 0.4	44.7 0.6	1.1	-30.6	15	773.9 0.4	619.9 1.0	1.1
-41.0	98	205.9 0.6	-329.6 0.4	1.5	-28.0	7	775.0 2.6	620.3 1.9	0.8
-40.8	47	386.4 0.5	363.7 0.3	0.4					

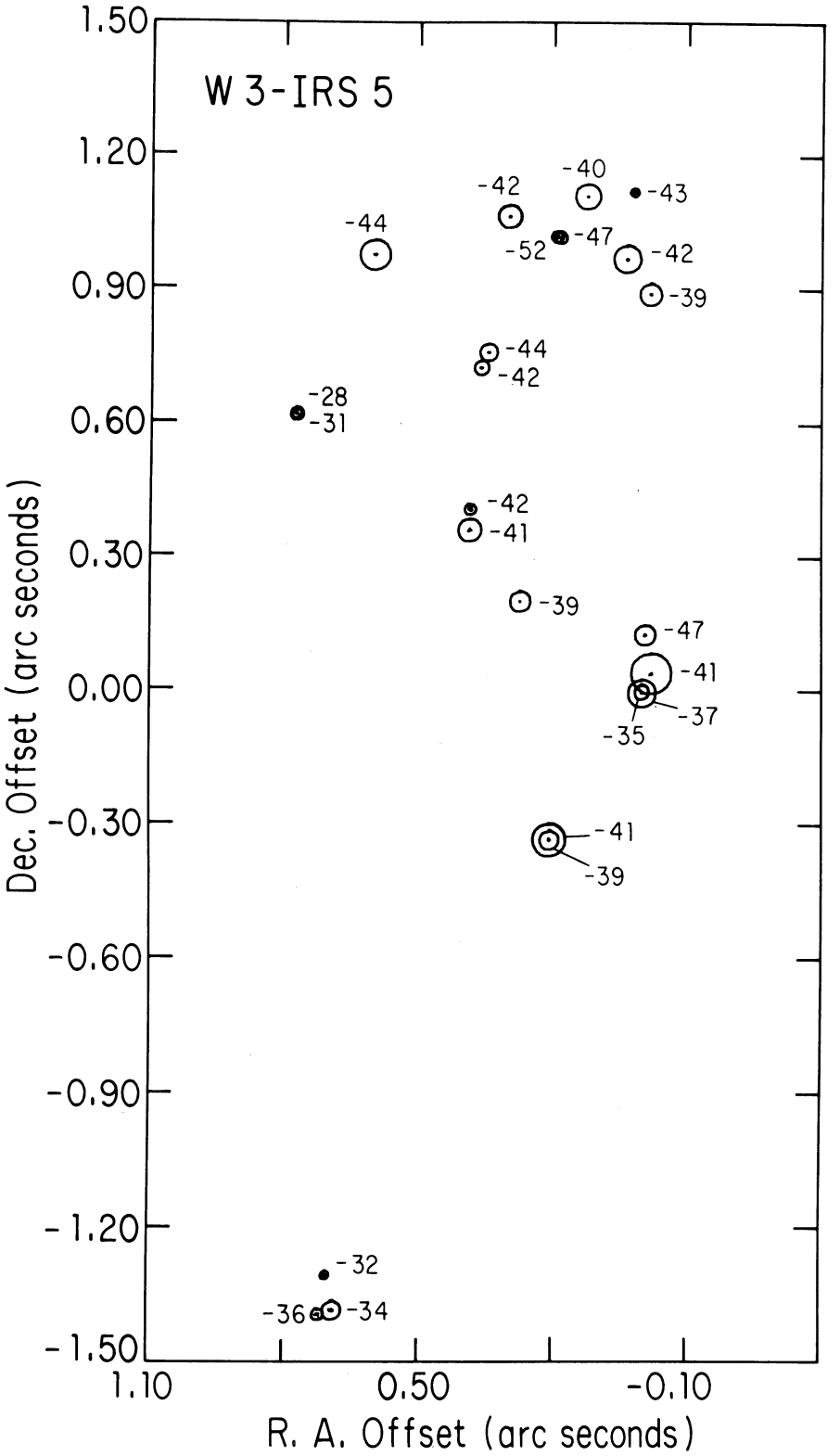

FIG. 5. The map of H_2O masers in W3–IRS5. Each feature is marked by a circle whose area is proportional to its flux density and by a cross, the arms of which indicate the one sigma errors in the feature position.

(Werner *et al.* 1980) with a total luminosity of $2\times10^5\,L_\odot$. Speckle interferometry results in the near infrared show that it is a double with a separation of about 1 arcsec (Low 1980). Radio observations at 15 GHz (Colley 1980) show that a 7-mJy continuum source lies about 1 arcsec east of the H_2O masers. The high total luminosity and weak radio emission indicate that IRS5 is a newly formed O star. If the star is located at the position of the radio source, it lies about 10^{17} cm from the masers, which is comparable to the size of the maser region. It is also possible that the radio source marks the most evolved of several newly formed stars (perhaps 2, as indicated by the infrared double) and that the possible clusters of masers mark separate objects. In any case, the association of a bright infrared object that has weak radio emission with H_2O masers supports the current belief that interstellar H_2O masers occur in disturbed regions of dense molecular gas surrounding newly formed OB stars (cf. Genzel *et al.* 1978).

IV. CONCLUSIONS

The multiple-point fringe-rate method of mapping spectral-line VLBI sources is a useful tool with which to study objects which consist of a small number of point sources at each velocity. This type of structure is typical of astrophysical masers. The ability to deal with more than one point at each frequency makes it much more accurate and reliable than the older single-point fringe-rate method. The tolerance of phase slopes due to clock errors and the avoidance of a map grid make it much easier to use than aperture synthesis. When the method is used, various limitations must be understood. As with any fringe-rate method used to date, the individual sources are assumed to be points. When a feature is partially resolved, its total flux density in the map will be reduced. The ability to separate close features is not nearly as good as with aperture synthesis, because the relative fringe rates of features only a few fringe spacings apart may be less than the fringe-rate resolution of each scan. The spatial window over which good positions can be obtained is limited by smearing of fringe-rate peaks, and is a function of integration time. Finally, the automatic program for finding features must be checked to avoid spurious features. The inability to separate features that are only a few fringe spacings apart is a severe problem for observations of OH masers at 18 cm, where the fringe spacings are large. The method is most useful for observations of H_2O masers at 1.35 cm, where the fringe spacings are small and where full calibration for aperture synthesis is much more difficult than at 18 cm.

Maps of the H_2O masers in W3(OH) and W3–IRS5 were presented which demonstrate the use of the method. These maps show significantly more features than single-point fringe-rate maps, especially in W3(OH), where there is much confusion. The wide distribution of features in both sources makes division into centers of activity difficult and suggests that each source is excited by a single energy source, presumably a newly formed, massive star. A similar conclusion is suggested for the far larger and more complex source, W49N, by a 386-point map presented in Paper I.

I wish to thank F. Isreal, B. Allen, B. Burke, J. Moran, and S. Lichten for assistance before and during the observations. I especially thank D. N. Matsakis for his efforts in installing a Berkeley maser on the Owens Valley Radio Observatory (OVRO) telescope and J. A. Garcia-Barreto for his help during the observations and data processing. I also thank the staffs of the observatories and of NRAO, in Charlottesville, for their support. I gratefully acknowledge the support of the OVRO during much of this work. VLBI research at OVRO and at Haystack Observatory is supported by the National Science Foundation.

REFERENCES

Burke, D. F., Giuffrida, T. S., and Haschick, A. D. (1978). Astrophys. J. Lett. **226**, L21.

Clark, B. G. (1973). Proc. IEEE **61**, 1242.

Colley, D. (1980). Mon. Not. R. Astron. Soc. **193**, 495.

Genzel, R., Downes, D., Moran, J. M., Johnston, K. J., Spencer, J. H., Walker, R. C., Haschick, A., Matveyenko, L. I., Kogan, L. R., Kostenko, V. I., Ronnang, B., Rydbeck, O. E. H., and Moiseev, I. G. (1978). Astron. Astrophys. **66**, 13.

Giuffrida, T. S. (1977). Ph.D. thesis, Massachusetts Institute of Technology.

Haschick, A. D., Burke, B. F., and Spencer, J. H. (1977). Science **198**, 1153.

Haschick, A. D., Reid, M. J., Burke, B. F., Moran, J. M., and Miller, G. (1981). Astrophys. J. **244**, 76.

Low, F. (1980). In *Optical and Infrared Telescopes of the 1990's*, edited by A. Hewitt (Kitt Peak National Observatory, Tucson), Vol. 2, p. 825.

Moran, J. M. (1973). Proc. IEEE **61**, 1236.

Moran, J. M. (1976). In *Methods of Experimental Physics*, edited by M. L. Meeks (Academic, New York), Vol. 12C, p. 228.

Reid, M. J., Muhleman, D. O., Moran, J. M., Johnston, K. J., and Schwartz, P. R. (1977). Astrophys. J. **214**, 60.

Reid, M. J., and Muhleman, D. O. (1978). Astrophys. J. **220**, 229.

Reid, M. J., Haschick, A. D., Burke, B. F., Moran, J. M., Johnston, K. J., and Swenson, G. W. (1980). Astrophys. J. **239**, 89.

Walker, R. C., Burke, B. F., Haschick, A. D., Crane, P. C., Moran, J. M., Johnston, K. J., Lo, K. Y., Yen, J. L., Broten, N. W., Legg, T. H., Greisen, E. W., and Hansen, S. S. (1978). Astrophys. J. **220**, 229.

Walker, R. C., Matsakis, D. W., and Garcia-Barreto, J. A. (1981). Submitted to Astrophys. J. (Paper I).

Werner, M. W., Becklin, E. E., Gatley, I., Neugebauer, G., Sellgren, K., Thronson, H. A., Harper, D. A., Loewenstein, R., and Moseley, S. H. (1980). Astrophys. J. **242**, 601.